XVII. PLASMA MAGNETOHYDRODYNAMICS AND ENERGY CONVERSION*

Prof. G. A. Brown
Prof. E. N. Carabateas
Prof. R. S. Cooper
Prof. S. I. Freedman
Prof. W. H. Heiser
Prof. M. A. Hoffman
Prof. W. D. Jackson
Prof. J. L. Kerrebrock
Prof. J. E. McCune
Prof. H. P. Meissner
Prof. J. R. Melcher
Prof. G. C. Oates
Prof. J. P. Penhune
Prof. J. M. Reynolds III
Prof. A. H. Shapiro
Prof. J. L. Smith, Jr.
Prof. R. E. Stickney
Prof. H. H. Woodson

Dr. A. T. Lewis
M. T. Badrawi
J. F. Carson
A. N. Chandra
J. M. Crowley
R. Dethlefsen
M. G. A. Drouet
D. A. East
R. K. Edwards
J. R. Ellis, Jr.
F. W. Fraim IV
J. W. Gadzuk
J. Gerstmann
J. B. Heywood
P. G. Katona
F. D. Ketterer
G. B. Kliman

A. G. F. Kniazzeh
M. F. Koskinen
K. S. Lee
R. F. Lercari
W. H. Levison
B. T. Lubin
S. A. Okereke
J. H. Olsen
E. S. Pierson
R. P. Porter
D. H. Pruslin
C. W. Rook, Jr.
A. W. Rowe
A. Shavit
A. Solbes
J. S. Weingrad
G. L. Wilson
J. C. Wissmiller

RESEARCH OBJECTIVES AND SUMMARY OF RESEARCH

1. Magnetohydrodynamics

Our work in magnetohydrodynamics is broadly concerned with the interactions between electromagnetic fields and electrically conducting fluids, particularly in those situations to which a continuum fluid description is applicable. Both plasmas and liquid metals are employed in the experimental aspects of our work and the development of measurement techniques receives particular attention. An important extension of this activity is the study of blood flow and related topics in biomedical engineering.

(a) Plasma Magnetohydrodynamics

The past year has been spent in improving the capabilities of the magnetic annular shock tube for producing clearly defined quantities of shock-heated gas and for measuring values of the physical quantities relevant to the experiments. These improvements are based upon experience with the original version of the shock tube. In particular, the following changes have been made:

(i) The duration and magnitude of the pre-ionization current have been increased to improve initial gas breakdown.

(ii) The sinusoidal drive current has been replaced by a square pulse to reduce time-variant effects.

(iii) All low-melting-point insulating materials have been removed, or covered with Pyrex, to reduce ablation from the surface of these insulators.

(iv) Eight magnetic field coils have been inserted around the annulus to measure the azimuthal distribution of drive current.

(v) A magnetic field coil has been provided to measure the variation of azimuthal magnetic field with time at a fixed axial position.

*This work was supported in part by the U. S. Air Force (Aeronautical Systems Division) under Contract AF33 (615)-1083 with the Air Force Aero Propulsion Laboratory, Wright-Patterson Air Force Base, Ohio; and in part by the National Science Foundation (Grant G-24073).

(vi) An electrostatic probe to complement the azimuthal magnetic field probe is being designed.

Experiments have begun and the results of these changes should soon be known. These experiments are particularly designed to test the azimuthal uniformity of the drive current. The long-range goals of these experiments are still the improvement of this type of shock tube and the careful investigation of magnetohydrodynamic shock waves.

A. H. Shapiro, W. H. Heiser, J. B. Heywood

(b) Mathematical Methods in Continuum Magnetohydrodynamics

This research is concerned with mathematical methods for the analysis of the interactions occurring in magnetohydrodynamics. The present work has grown out of the investigation of MHD channel flows; particularly out of the analytical and numerical techniques that were used to obtain solutions to the nonlinear differential equation governing the interaction of a traveling AC magnetic field with an MHD channel flow.

Our research concerns the application of techniques, such as perturbation expansions and iterational and variational methods, to a variety of nonlinear continuum MHD problems. The purpose of this effort is twofold: first, to produce solutions to specific problems that are of practical interest; second, to obtain a better understanding of the broad classes of problems to which these techniques are applicable. The analysis of the flow of an electrically conducting fluid around a sphere with a dipole magnetic field is at present being undertaken for the case in which the dipole axis is perpendicular to the direction of fluid flow.

J. P. Penhune

(c) Magnetohydrodynamic Wave Phenomena

One of our experiments is concerned with the excitation of Alfvén waves in a liquid metal (NaK alloy). Generation of these waves by using a current-sheet excitation has been verified, and shown to be markedly superior to the mechanical methods used in experiments reported previously. The systematic study of the excitation transmission, attenuation, and reflection of these waves in the hydromagnetic waveguide continues.

A second waveguide study is concerned with MHD wave propagation in nonuniform magnetic fields. NaK alloy again serves as the working fluid for the experimental part of this investigation.

A theoretical study of MHD surface waves on fluids of finite electrical conductivity is also being undertaken. An experimental study of some aspects of these waves has recently been initiated, and will also use NaK as the working fluid.

W. D. Jackson, J. P. Penhune

(d) Magnetohydrodynamic Channel Flow and Turbulence

The flow characteristics of electrically conducting fluids in channels or ducts are of interest in connection with many engineering applications of magnetohydrodynamics. While these include both liquid and ionized gas flows, the use of liquid metals has advantages for a considerable range of laboratory investigations.

A closed-loop flow facility has been constructed with NaK used as the working fluid. This loop is being used for study of pressure drop versus flow-rate relations (including those for MHD power-conversion devices), and the characteristics of turbulence in the presence of magnetic fields.

The character of MHD turbulence is modified when a pronounced Hall effect occurs in the flow. The characteristics of turbulence in this situation are being investigated,

and work continues on the application of Norbert Wiener's "Calculus of Random Functionals" to the study of turbulent-flow situations.

W. D. Jackson

(e) Local Fluid-Velocity Measurement in an Incompressible Magnetohydrodynamic Flow

The behavior of different types of velocity probes is being investigated to develop devices capable of measuring the local fluid velocity in an MHD flow for the case in which the applied magnetic field is perpendicular to the fluid velocity. The development of such probes will be important for experimental investigation of MHD flows, particularly those associated with MHD power-generation schemes.

The behavior of a nonconducting Pitot tube is being investigated experimentally. Here the $\underline{J} \times \underline{B}$ forces increase the pressure measured at the stagnation point above the usual stagnation pressure. The velocity-pressure correlation has been determined experimentally as a function of applied magnetic field for a probe with a flat front end perpendicular to the axis of the tube. The effects of probe angle of attack and nose shape are now being studied.

A miniaturized electromagnetic flowmeter is also receiving attention.

A feasibility study is being made to determine whether a hot-wire anemometer can be constructed with sufficient sensitivity to be useful in the sodium-potassium eutectic liquid-metal flow loop described in (d) above.

A. H. Shapiro, W. D. Jackson, R. S. Cooper, D. A. East

(f) Ionization Waves in Weakly Ionized Plasmas

During the past year, some further studies have been made on the nature of certain macroscopic instabilities observed in the plasma of glow discharge tubes. The region of tube operation in which the instability is incipient has been defined for several gases, and the properties of shock-excited waves generated by external sources have been thoroughly examined in these regions.

Further work is being done toward the development of a theory to describe the behavior exhibited by the plasma in these experiments. Some new experiments are being performed to find additional methods of exciting the observed ionization waves. The interaction of the waves with internally generated sonic waves in the neutral gas is also being investigated both experimentally and theoretically.

R. S. Cooper

(g) Blood-Flow Studies*

Electrical methods are widely used in blood-flow measurement, and prominent among the devices used is the magnetohydrodynamic or electromagnetic flowmeter. Work reported under (e) above is being adapted for both mean and local blood-flow measurement and magnetohydrodynamic, thermal, and ultrasonic techniques are at present under investigation.

A second aspect of our blood-flow work is concerned with the application of engineering methods to the study of the cardiovascular system. We are engaged in this research jointly with Dr. Dexter and his associates at Peter Bent Brigham Hospital. A study of the pressoreceptor system has recently been completed as a step in the

*This work is supported in part by the National Institutes of Health (Grant No. 5 TI HE 5550-02).

identification and analysis of the mechanisms responsible for the regulation of cardiovascular functions.

G. O. Barnett,* W. D. Jackson

2. Energy Conversion

Our studies include both magnetohydrodynamic and thermionic methods of generating electrical power, and involve over-all system considerations, properties of working fluids, and operating characteristics of conversion devices.

(a) Magnetohydrodynamic Power Generation with Liquid Metals

The generation of electrical power in space vehicles offers a potential application for MHD generators to operate on a closed-cycle system in which a nuclear reactor is the thermal-energy source. An important feature of an MHD system is the absence of rotating parts, and, to utilize it, a working fluid is required with a sufficiently high electrical conductivity at the temperatures involved. A scheme in which a liquid metal is used as the working fluid in the MHD generator duct is under investigation. Kinetic energy is imparted to this flow by driving it with its own vapor in a condensing-ejector system.

A cycle analysis has been completed and has revealed efficiencies that are sufficiently attractive to warrant detailed investigation. During the coming year, the operation of condensing ejectors on alkali metals will be considered, the conductivity of two-phase flows in the presence of magnetic fields will be measured, the study of liquid-metal generator configurations will continue, and further cycle analysis will be performed.

W. D. Jackson, G. A. Brown

(b) Magnetohydrodynamic Induction Generator

The MHD induction machine utilizes the interaction between a traveling magnetic field (such as that produced by a polyphase winding) and a channeled, flowing fluid that may be either a plasma or a liquid metal.

The theoretical analysis of this machine has been extended to include such real machine effects as entry and exit conditions, finite core permeability, and velocity profile effects. This work has clearly demonstrated that the reactive power requirements of an induction generator are excessive when operated on a plasma flow but that satisfactory operation should be obtained with liquid metals.

A preliminary experimental investigation of a linear induction generator operating on an NaK flow with a two-phase, traveling-field coil system has demonstrated electrical power generation. This work will be extended and developed during the coming year.

W. D. Jackson

(c) Alkali-Metal Magnetohydrodynamic Generators

The over-all objective of this research is to investigate the feasibility of operating magnetohydrodynamic generators with alkali metals as working fluids. Our immediate objective is to establish the electrical properties of both superheated and wet alkali-metal vapor at temperatures up to 2000°K.

---

*Dr. G. O. Barnett is Established Investigator, American Heart Associate, Harvard Medical School, Boston, Massachusetts.

A small potassium loop, capable of a mass flow of 10 grams per second, has been constructed and is now being put into operation. Meanwhile, analytical studies of the wet vapor have been carried to the stage at which electrical conductivities can be computed, if the distribution in size of the droplets can be determined.

J. L. Kerrebrock

(d) Thermionic Energy Conversion

The research objectives of our group are oriented toward the evaluation of possible improvements of thermionic-converter performance based on the recent developments in the areas of surface and transport effects. The following studies are at present being conducted:

(i) Parametric evaluation of ideal converter performance as determined by the properties of cesium films on polycrystalline and single-crystal metallic surfaces.

(ii) Detailed study of the processes responsible for the creation of the highly conducting plasma in the interelectrode region of cesium thermionic converters, and interpretation of experimental current-voltage characteristics in the ignited mode.

(iii) Extension of previous measurements of the thermal conductivity of cesium vapor to higher temperatures and possibly to other alkali metals.

E. N. Carabateas

(e) A-C Properties of Superconductors

Recent intensive efforts to fabricate hard superconductors have opened up a wide range of possibilities for utilizing these materials in the production of high DC fields, particularly in situations for which these are required in large volume. The advantages associated with reducing field-power dissipation also apply to the production of AC fields, but there is an additional problem in that reactive power has to be circulated. This problem essentially implies zero-loss capacitive energy-storage elements, in addition to essentially infinite Q inductors. It is thus of interest to investigate the behavior of superconducting materials carrying AC currents in the presence of AC magnetic fields. As well as establishing the merits of superconducting materials in inductor and capacitor fabrication, such investigations provide an additional method of gaining insight into the mechanism of superconductivity.

Present investigations deal with superconducting materials in the form of wire or ribbon, and two experimental techniques are being pursued.

(i) The current-carrying capacities of short, straight lengths of superconducting wire or ribbon are being determined as a function of frequency in the range up to 10 kc.

(ii) A-C solenoids, fabricated to avoid electric eddy currents and insulated to accommodate electrical fields arising from $\partial B/\partial T$ effects, are being tested. In both cases, the AC current required for transition to normal conductivity has been obtained and, in the case of solenoids, the Q has been measured.

A third investigation is planned to obtain data on the behavior of superconductors in an externally applied AC field. These data will be derived either from a rotating magnet system or from a separate copper-conductor AC solenoid.

The work is, at present, experimental in character, but future theoretical studies are envisaged.

W. D. Jackson

(XVII. PLASMA MAGNETOHYDRODYNAMICS)

A. WORK COMPLETED

1. LARGE-SIGNAL BEHAVIOR OF A PARAMETRIC MAGNETOGASDYNAMIC GENERATOR

This report summarizes an Sc. D. thesis with this title which was submitted to the Department of Electrical Engineering, M. I. T., September 20, 1963, and will appear as an RTD Technical Documentary Report

In this study the large-signal behavior of a parametric magnetogasdynamic generator, consisting of a cylindrical coil with batches of highly conducting plasma traveling along the coil axis, is considered. In this limit, the gas behavior is strongly affected by the magnetic forces. The purpose of this study was to determine (i) whether the requirements on the conductivity and velocity of the gas found for small-signal behavior are relaxed because of any enhancing mechanism during the interaction; (ii) what fraction of the gas power could be extracted as useful electrical power, that is, the over-all generator efficiency; (iii) how the interaction between the field and the gas leads to gas behavior that limits the growth of the parametric oscillations so that a stable operating point is reached; (iv) an estimate of the minimum size and power of a generator with present technology; and (v) the factors that control the scaling of the parametric generator.

To answer these questions, an analysis is presented for the small-signal behavior to establish the important parameters and provide a basis of comparison for the large-signal behavior. The large-signal electrical and gas behavior are treated separately as far as possible. A criterion is established for determining the steady-state operating point in terms of the electrical terminal behavior. The gas-flow interaction with the field is analyzed by using a quasi one-dimensional-flow model with the constraints for a strong interaction that the magnetic pressure balance the static gas pressure in the radial direction, and the power given up by the gas balance the gross electrical power generated.

A. T. Lewis

B. ALFVÉN WAVE STUDIES

1. SOME PROPERTIES OF MAGNETOHYDRODYNAMIC WAVEGUIDES

The dispersion equation for the MHD waveguide has been derived by a number of investigators.[1-7] Basically, the MHD waveguide consists of a hollow, rigid-wall cylinder of arbitrary, but constant, cross section immersed in a uniform, steady magnetic field aligned parallel to the cylinder axis as in Fig. XVII-1, and filled with a homogeneous electrically conducting fluid.

The total behavior of such a waveguide may be described in terms of transverse

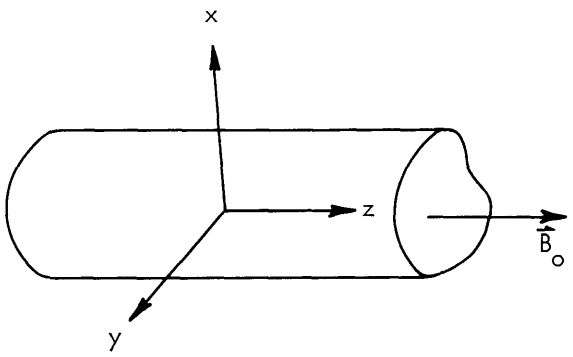

Fig. XVII-1. Coordinate system for the MHD waveguide.

magnetic (TM) and transverse electric (TE) modes. In general, any wave propagated consists of infinite sums of the two types of modes. In particular, if the fluid is inviscid and if the cross section and excitation are symmetric, single modes may be excited.[7]

In most magnetohydrodynamic waveguide problems, the critical fluid properties are the mass density and the electrical conductivity. Thus viscosity and displacement are neglected. Also, the modes of greatest interest are the TM modes and these do not compress the fluid, so that compressibility may also be neglected.

The resultant differential equation for the TM modes is

$$\nabla_t^2 e_z + T_{mn} e_z = 0, \tag{1}$$

where e_z is the longitudinal component of the electric field, and ∇_t^2 is the transverse Laplacian operator. Other symbols are defined as follows:

$$T_{mn}^2 = \frac{C^2 + i\omega\eta_t}{i\omega\eta_\ell}\left(\frac{\omega^2}{C^2 + i\omega\eta_t} - \beta_{mn}^2\right), \tag{2}$$

where the propagation has been taken as $e^{i(\omega t+\beta_{mn}z)}$;

$$C^2 = \frac{B_o^2}{\mu_o\rho} = \text{Alfvén velocity;}$$

$$\eta_\ell = \frac{1}{\mu_o\sigma_\ell} = \text{longitudinal magnetic diffusivity;}$$

$$\eta_t = \frac{1}{\mu_o\sigma_t} = \text{transverse magnetic diffusivity;}$$

with B_o, the magnitude of the applied magnetic field; ρ, the mass density of the fluid; σ_ℓ, the longitudinal electric conductivity; σ_t, the transverse electric conductivity; and μ_o, the permittivity of free space.

The solutions of (1) in rectangular coordinates are sinusoids and yield[8]

$$T_{mn}^2 = (2m+1)^2\left(\frac{\pi}{2a}\right)^2 + (2n+1)^2\left(\frac{\pi}{2b}\right)^2. \tag{3}$$

Here, a and b are the half-widths of a rectangular waveguide. In cylindrical coordinates the solutions of (1) are Bessel functions and yield

$$T_{mn}^2 = \left(\frac{\alpha_{mn}}{a}\right)^2. \tag{4}$$

Here, a is the radius of a cylindrical waveguide, and α_{mn} is the n^{th} root of the m^{th}-order Bessel function.

The propagation constant β is obtained from (2).

$$\beta_{mn}^2 = -\frac{\eta_\ell}{\eta_t}\,\frac{T_{mn}^2 + i\omega/\eta_\ell}{1 + C^2/i\omega\eta_t}. \tag{5}$$

At very low frequencies ($\omega \to 0$) (5) becomes

$$\beta_{mn} = \frac{T_{mn}}{c}\sqrt{\frac{\omega\eta_\ell}{2}}\,(1-i). \tag{6}$$

At very high frequencies ($\omega \to \infty$) (5) becomes

$$\beta_{mn} = \sqrt{\frac{\omega}{2\eta_t}}\,(1-i). \tag{7}$$

At intermediate frequencies such that

$$\eta_\ell T_{mn}^2 \ll \omega \ll C^2/\eta_t, \tag{8}$$

(5) becomes approximately

$$\beta_{mn} = \left(\frac{\omega}{c}\right)\left[1 - \frac{i}{2}\left(\frac{\omega\eta_t}{c^2} + \frac{T_{mn}^2}{\omega}\eta_\ell\right)\right]. \tag{9}$$

Equations 6 and 7 are characteristic of diffusion phenomena. At low frequencies the magnetic field diffuses through the fluid in a time short compared with the period of the excitation. Thus the field is not convected by the fluid. At high frequencies the field cannot penetrate the fluid. Thus the fluid is not convected by the field. But if ω satisfies (9), there is a region in which mutual convection of the fluid and the field gives rise to the Alfvén wave.

If the asymptotes of Re (β) and -Im (β) in (6), (7), and (9) are plotted in log-log coordinates, Fig. XVII-2 results. An exact evaluation of (5) for a shock-excited gas experiment is also plotted in Fig. XVII-2, and shows that the asymptotes are a very good approximation to the exact curves.

The intersections of the asymptotes are interesting points, two of which correspond to condition (8). Notice that the lower limit of the Alfvén region is controlled

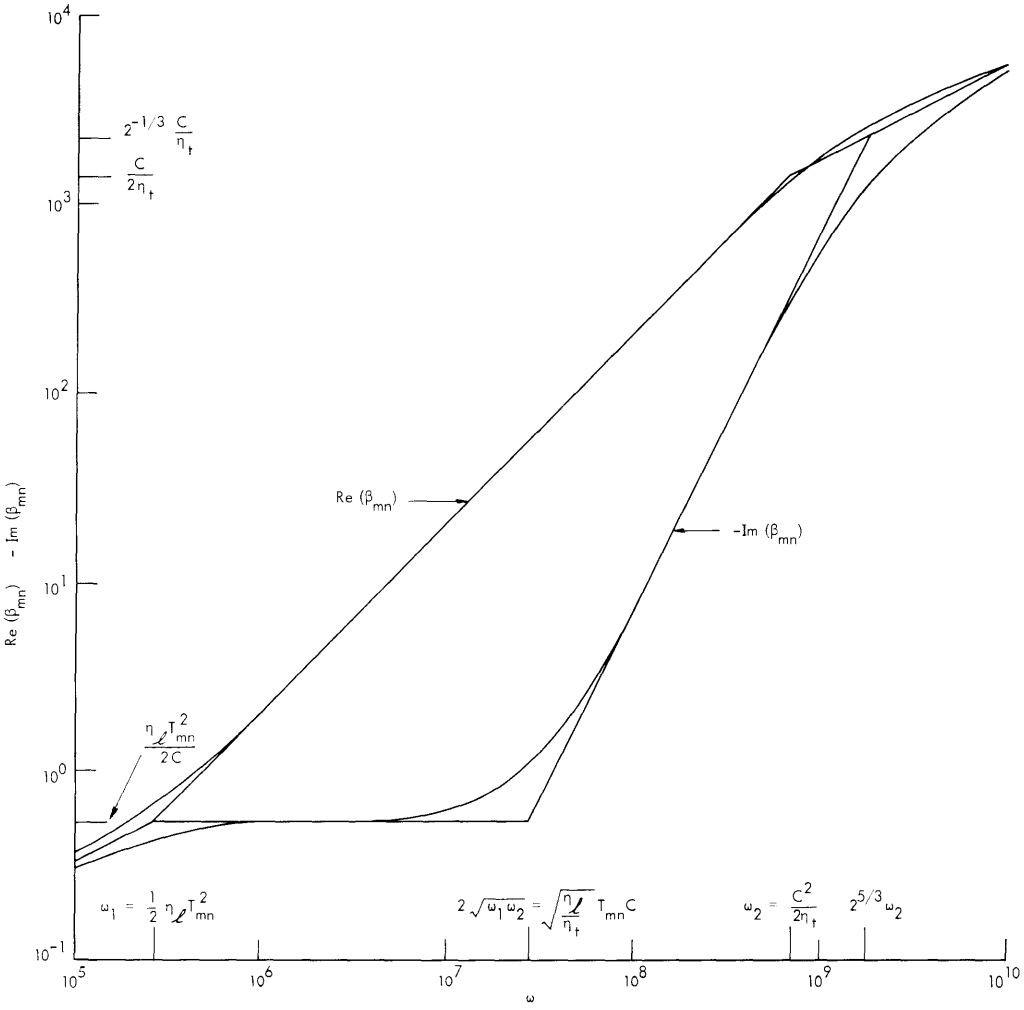

Fig. XVII-2. Typical shock-excited gas experiment.
$\sigma_\ell = \sigma_t = 4.5 \times 10^3$ v/m (Te = 3.5 ev); $\rho = 1.7 \times 10^{-5}$ kg/m^3 (n = 1.5×10^{15}/cc H^+); B_o = 1.6 w/m^2; b = 0.07 m; T_{01} = 3.8/b (J_1(Tb) = 0); Va = 5×10^5 m/sec; $\eta_\ell = \eta_t = 1.8 \times 10^2$ m^2/sec; $\omega_2/\omega_1 = 2.6 \times 10^3$.

by conductivity and geometry, while the upper limit is controlled by conductivity, density, and applied field. The frequency below which, under condition (8), the waveguide is distortionless is twice the geometric mean of the upper and lower

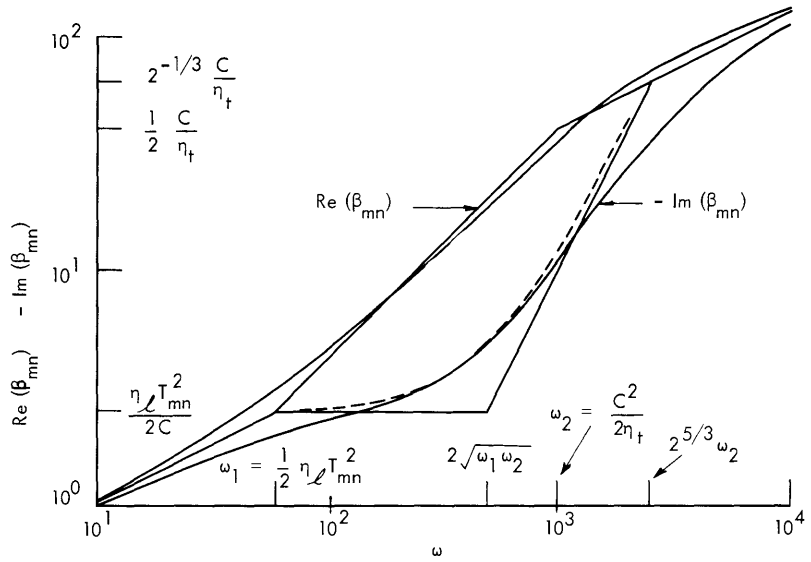

Fig. XVII-3. Typical liquid-metal experiment.
$\sigma_\ell = \sigma_t = 2.63 \times 10^6$ v/m; $\rho = 8.5 \times 10^2$ kg/m^3 (NaK);
$B_o = 0.8$ w/m^2; b = 0.19 m; $T_{01} = 3.8/b$ ($J_1(Tb) = 0$);
Va = 24.5 m/sec; $\eta_\ell = \eta_t = 0.3$ m^2/sec; $\omega_2/\omega_1 = 16$.

limits. In Fig. XVII-3 data are plotted for a typical liquid-metal experiment for comparison.

In view of these results, Eq. 5 should be rewritten

$$\beta_{mn}^2 = \left(\frac{\omega}{c}\right)^2 \frac{1 - 2i\frac{\omega_1}{\omega}}{1 + \frac{1}{2i}\frac{\omega}{\omega_2}}. \tag{10}$$

Now,

$$\frac{\omega}{2\omega_1} = \frac{\omega}{\eta_\ell T_{mn}^2} = \text{magnetic Reynolds number}$$

$$\frac{2\omega_2}{\omega} = \frac{C^2}{\omega\eta_t} = \text{Lundquist number.}$$

Thus, in order that an Alfvén wave exist, both the magnetic Reynolds and Lundquist numbers must be large compared with unity.

Listed below in tabular form is a comparison of a number of Alfvén wave experiments in terms of the critical frequencies.

	Experimenter	Medium	f_1	f_2
1.	Jephcott, Stocker, and Woods[4]	arc plasma	46.5 kc	51.3 mc
2.	Wilcox, da Silva, Cooper, and Boley[3]	shock plasma	41.4 kc	111.0 mc
3.	DeCourey and Bruce[9]	irradiated gas	57.2 mc	4.07 mc
4.	Gothard,[8] and Jackson and Carson*	NaK	9.75 cps	158 cps
5.	Lundquist[1]	Hg	159 cps	10.3 cps
6.	Lehnert[2]	Na	21.5 cps	770 cps

*See W. D. Jackson and J. F. Carson (Sec. XVII-B2).

G. B. Kliman

References

1. S. Lundquist, Phys. Rev. 83, 307 (1951).

2. B. Lehnert, Phys. Rev. 94, 815 (1954).

3. J. M. Wilcox, A. W. da Silva, W. S. Cooper, and F. I. Boley, Experiments on Alfvén Wave Propagation, in Radiation and Waves in Plasma, edited by M. Mitchner (Stanford University Press, 1961), p. 138.

4. D. F. Jephcott, P. M. Stocker, and L. C. Woods, IAEA Report CN-10/62, 1962.

5. R. W. Gould, STL Report TR-60-0000-09143, 1960.

6. J. Shmoys and E. Mishkin, Phys. Fluids 3, 473 (1960).

7. L. C. Woods, UKEA Research Group Report CLM-R5, 1961.

8. N. Gothard, S. M. Thesis, Department of Electrical Engineering, M. I. T., 1962.

9. D. J. DeCourey, Jr. and M. H. Bruce, Report AFCRL G2-550, 1962.

2. EXPERIMENTS WITH A LIQUID-METAL MAGNETOHYDRODYNAMIC WAVEGUIDE

The presence of hydromagnetic waves in conducting fluids was first established by Alfvén,[1] in 1942. Since that time, much progress has been made in the theoretical study of these waves, but experimental work has proceeded slowly. Lundquist,[2] in 1951, tried to excite waves in mercury, and Lehnert[3] repeated and improved the experiment, in 1954, using liquid sodium. Other experimental work has been done

with shock-excited plasmas.[4,5] Most of the results thus far have been somewhat inconclusive, showing only partial agreement with theoretical predictions.

Many of the difficulties in experimental work have been caused by the need for a high-conductivity working fluid to avoid excessive attenuation. The Lundquist number, a reciprocal magnetic Reynolds number based on Alfvén velocity and wavelength, is defined as

$$Lu = \frac{2\pi f}{B_o^2}\left(\frac{\rho}{\sigma}\right),$$

where f is the excitation frequency, B_o the applied magnetic field, ρ the fluid density, and σ the fluid electrical conductivity. It provides a convenient basis on which the suitability of a medium may be established and, to ensure propagation without undue attenuation, it must be much less than one, which in turn requires that the ratio of electrical conductivity to mass density be as large as possible. Lehnert was able to achieve improvement in the Lundquist number of over 100 by using sodium instead of mercury. Handling and instrumentation problems are always present in alkali-metal research, and the high temperature necessary to liquify sodium leads to additional complications. The use of sodium-potassium eutectic alloy as the working fluid affords an increase over mercury in the conductivity-density ratio about three times less than that of pure sodium. Sodium potassium affords the advantage of being liquid at room temperature, and accordingly has been chosen as the working fluid for this experiment.

Lundquist attempted to launch waves, using a vibrating disk with vanes attached. The device was intended to couple mechanically to the fluid and to cause torsional disturbances that would propagate along the axial magnetic-field lines, but the mechanism at work was really motional induction. Therefore Lehnert used a copper disk without vanes. The rotation of the disk in the magnetic field caused an induced electric field in the disk. Matching of tangential electric-field components across a boundary requires an induced current to flow in the fluid. This current in turn reacts with the magnetic field to form a $\overline{J} \times \overline{B}$ force that acts on the fluid to generate vorticity and, if conditions permit, the vorticity will propagate.

The search for an optimal means of excitation led to the use of a directly injected current sheet to launch the waves. A small disk, 5 cm in diameter, in the center of the waveguide shown in Fig. XVII-4 is fed with alternating current. A copper collecting ring soldered to the outside wall of the waveguide provides a return. The feed conductors leading from the ring to the source are designed to give equal resistance in all paths, and result in a reasonably symmetrical current-sheet excitation. Exciting currents are of the order of 100 amps.

The waveguide itself is constructed of stainless steel, and has an internal diameter

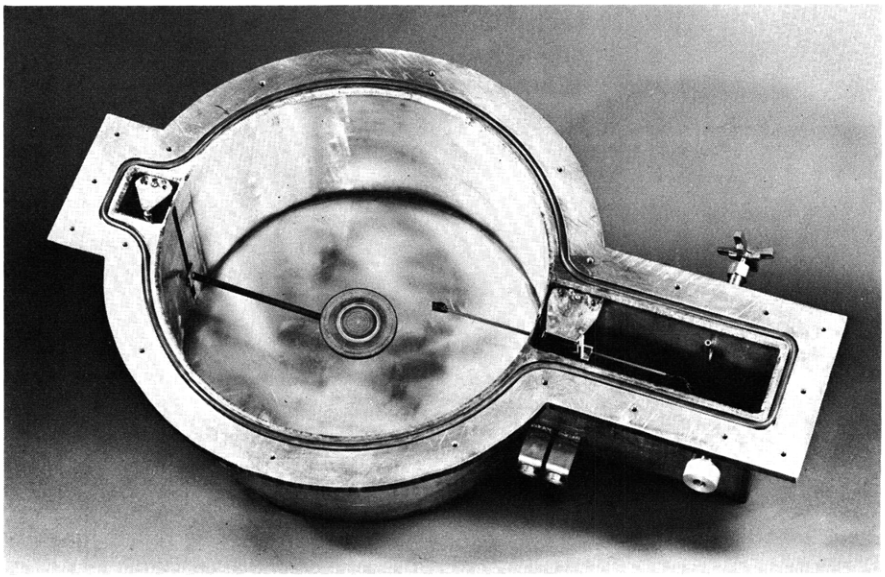

Fig. XVII-4. MHD waveguide showing excitation structure.

of 38 cm. The length of the waveguide is 18 cm, and is limited by the gap length of the magnet that was available. The applied magnetic field is 0.8 weber/meter^2. The rectangular chamber on the left of the waveguide contains the elevating mechanism for the exciter probe. With this arrangement it is possible to position the probe at any height within the waveguide. The chamber on the right contains the mechanism for both radial and axial movement of probes for local magnetic-field measurements. Counters attached to the shafts provide information about the location of the probes. The waveguide is filled and drained with the aid of a filling-station apparatus that contains the necessary valves and fittings for transferring the sodium potassium from storage cans to the waveguide.

If a sinusoidal drive and an $\exp(\bar{k} \cdot \bar{r})$ space dependence are assumed, the dispersion relation is obtained[6] from the pertinent hydrodynamic equations that yield values of the real and imaginary parts of the propagation vector as a function of frequency. The values of Alfvén speed v, wavelength λ, and attenuation α calculated for the conditions of the experimental apparatus are shown in Fig. XVII-5. The frequency dependence of v above ~200 cps indicates that this is a diffusion-controlled region and that waves should only be observed below this frequency. The method of excitation used in this experiment produced waves with magnetic-field components in the transverse plane only. The addition of a conducting center column would allow propagation of purely transverse electromagnetic waves.

Lundquist used a floating mirror to detect waves. Lehnert refined the measurement somewhat by measuring potential difference in the moving fluid with two probes. The approach taken in the present experiment was to look at the waveguide in as many ways

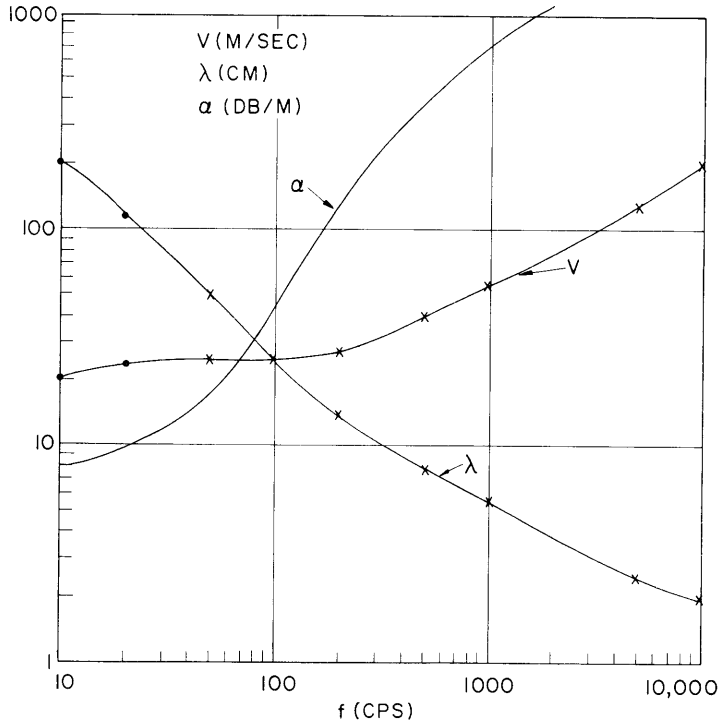

Fig. XVII-5. Wave properties as a function of frequency.

as possible. Two measurement schemes are possible when direct electric excitation is used. The relation of voltage and current at the driving terminals may be examined, and the internal fields of the waveguide may be measured. The field probe used for this experiment consisted of a solenoid, 3/8 in. in diameter, with 300 turns of number 37 wire. The coil was oriented so that the magnetic field induced in the ϕ direction was measured. The output of the probe was examined with an oscilloscope and voltmeter. A probe to measure local velocity in the fluid is under development, but was not available when the present experiment was performed.

Since the waveguide is of finite length, examination of the terminal impedance yields resonances. The results are shown in Fig. XVII-6 to be consistent with theoretical predictions based on calculated values of wavelength. The waveguide is essentially being run as a resonant cavity when operating at these points. The internal-field measurements were made at the resonances indicated on the impedance graph.

The measurements illustrated were taken with the exciter probe located at a height of 3 cm; this enabled the excitation of the $\lambda/2$ and $3\lambda/2$ resonances as indicated. Movement of the probe in the radial direction provided profiles of the type shown in Fig. XVII-7, while axial profiles obtained at a radius of 12 cm are given in Fig. XVII-8. To check that wave propagation was occurring, one set of data was obtained with a free surface at the top of the waveguide. Excitation without the applied field yielded a decay

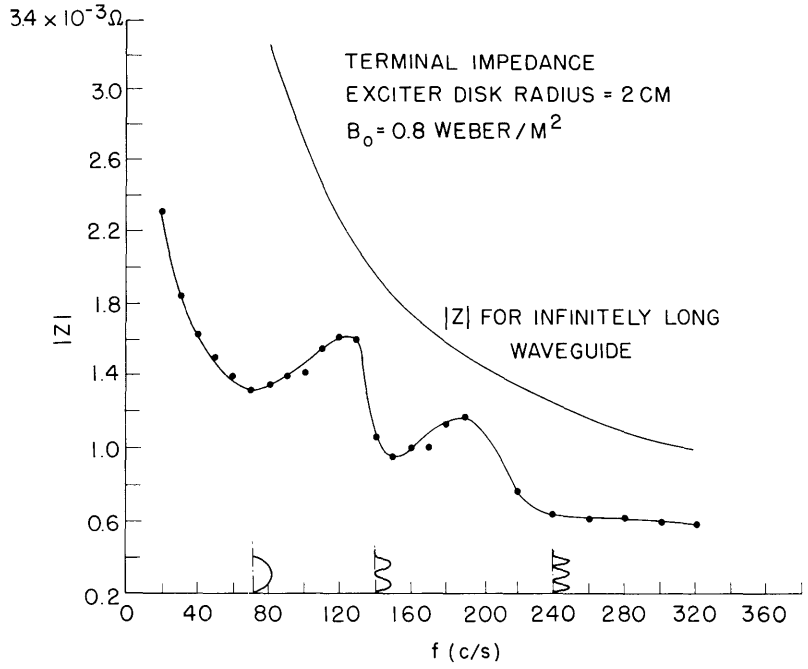

Fig. XVII-6. Resonance measurements.

of the induced field away from the exciter, while, with the field applied, an indication of free-surface motion was obtained as shown in Fig. XVII-8.

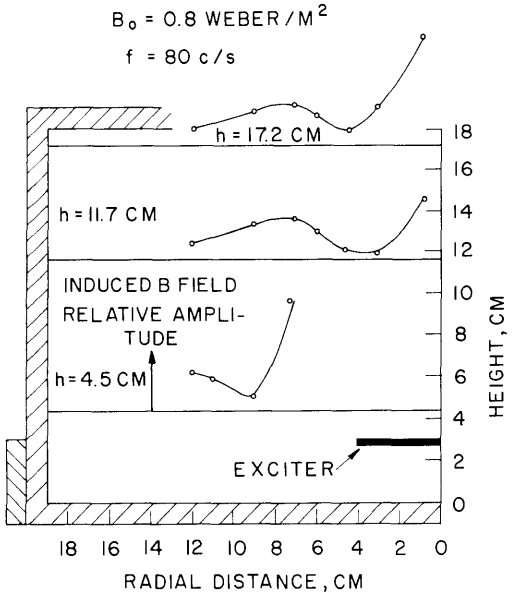

Fig. XVII-7. Induced B field — radial traverses.

The growth of the induced field along the axis is particularly evident in the case of the $3\lambda/2$ resonance, and is probably explained by the near-effects of the exciting-current sheet. The exciting disk was insulated on both top and bottom surfaces, and thus the fluid immediately above and below it is weakly coupled to the electromagnetic effects. The data of Fig. XVII-7 are consistent with the existence of a stationary volume of liquid above the exciter, but further experimental work is required to clarify the behavior in this region, and the waveguide is now being modified for this purpose.

The work reported here is of a preliminary nature, but it has served to indicate the feasibility of using a sodium-potassium

alloy as the working fluid in the study of Alfvén waves, as an alternative to the transient conditions of a shock-excited plasma. Conduction-type direct electrical excitation has been shown to be greatly superior to the vibrating disks used by early

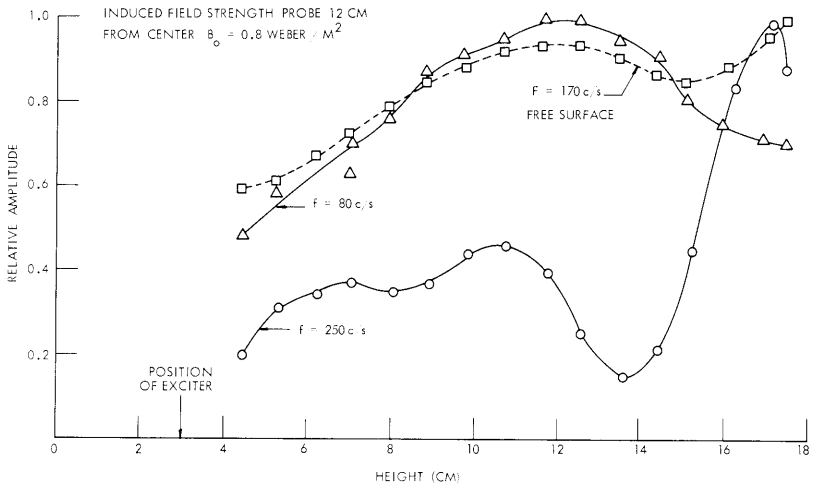

Fig. XVII-8. Induced B field – axial traverses.

experimenters, and magnetic field probes have proved to be satisfactory for the detection of wave conditions inside the waveguide. This study will continue, and will be concerned with both transverse magnetic and transverse electromagnetic modes, a different excitation, and different boundary conditions.

W. D. Jackson, J. F. Carson

References

1. H. Alfvén, Nature 150, 405 (1942).

2. S. Lundquist, Phys. Rev. 83, 307 (1951).

3. B. Lehnert, Phys. Rev. 94, 815 (1954).

4. J. M. Wilcox, A. W. da Silva, W. S. Cooper, and F. I. Boley, Experiments on Alfvén Wave Propagation, in Radiation and Waves in Plasma, edited by M. Mitchner (Stanford University Press, 1961), p. 138.

5. D. F. Jephcott, P. M. Stocker, and L. C. Woods, IAEA Report CN-10/62, 1962.

6. R. W. Gould, STL Report TR-60-0000-09143, 1960.

7. J. Shmoys and E. Mishkin, Phys. Fluids 3, 473 (1960).

8. L. C. Woods, UKEA Research Group Report CLM-R5, 1961.

9. N. Gothard, S. M. Thesis, Department of Electrical Engineering, M. I. T., 1962.

10. D. J. DeCourey, Jr. and M. H. Bruce, Report AFCRL G2-550, 1962.

C. MAGNETOHYDRODYNAMIC POWER GENERATION WITH LIQUID METALS

Preliminary studies on a liquid-metal MHD power system employing a condensing ejector have been completed. The objective was to determine the expected cycle efficiencies and specific weights by using available fluid-dynamic, thermodynamic, and

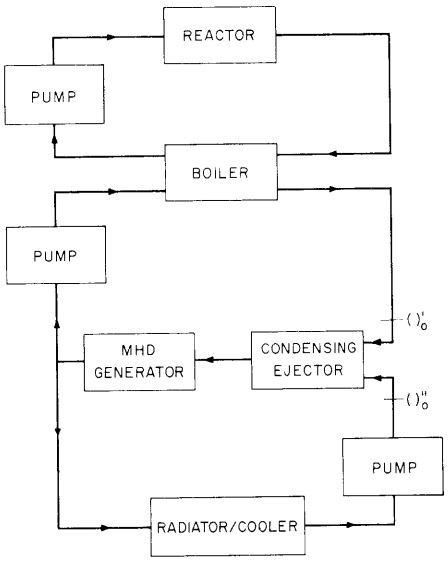

Fig. XVII-9. Liquid-metal MHD power system employing a condensing ejector.

heat-transfer information for the components and processes of the cycle. For the present, the liquid-metal MHD generator has been characterized as having a specified efficiency. Later studies will integrate the generator performance parameters with those of the components that are used to produce the liquid-metal stream in a complete system study.

The basic cycle is shown in Fig. XVII-9. Three loops are required for the conversion system. Energy from a nuclear reactor is transferred to a flowing liquid, perhaps lithium, which boils the primary working fluid, cesium, in the boiler section between the first and second loops. The cesium vapor then enters the condensing ejector at state $(\ )'_0$. The condensing ejector also receives "cool" liquid cesium, state $(\ )''_0$, which is returned from the radiator in the third loop. These two streams are mixed in the condensing ejector so as to produce a liquid-cesium stream having a high stagnation pressure. The liquid cesium stream is then split with a fraction being returned to the boiler and the remainder being returned to the radiator.

Available analytical and experimental data have been used to calculate the performance of the condensing ejector. Calculations have been made to establish the pressure drops and weights for the boiler and radiator, including state-of-the-art results for the two-phase flow, which occurs in the boiler under zero gravity conditions.

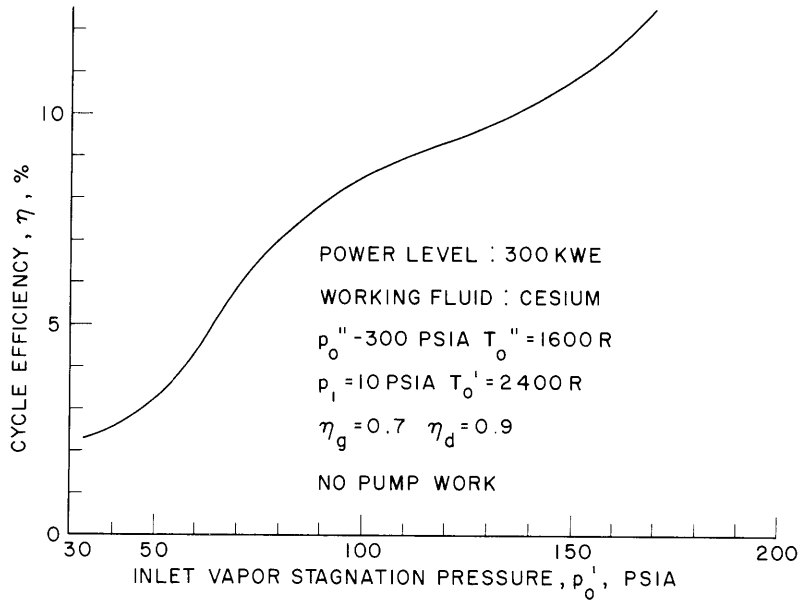

Fig. XVII-10. Effect of vapor stagnation pressure on cycle efficiency.

The cycle efficiency for the best conditions found thus far is shown in Fig. XVII-10. The conditions are for a space power system with a 300-kwe output. Cesium vapor is supplied to the condensing ejector at 2400 R and for the stagnation pressures shown in Fig. XVII-10. The cesium liquid enters at 1600 R and 300 psia. Both streams are then accelerated to a pressure of 10 psia in the condensing ejector. The liquid-cesium stream from the ejector is usually available at a high velocity, and can be diffused to any desired stagnation pressure before entry into the generator. A diffuser efficiency of 90 per cent has been used. A generator efficiency of 70 per cent has also been employed. The cycle efficiency is very low, approximately 2 per cent, when p_o'' is 30 psia, but increases steadily to approximately 12.5 per cent at 170 psia. The omission of the pump power for the reactor loop will drop the cycle efficiency by an increment of approximately 0.5 per cent.

Since the calculated cycle efficiencies and specific weights for the liquid-metal MHD power system are quite competitive with other systems now under consideration, further studies of it are planned.

G. A. Brown, W. D. Jackson, K. S. Lee

D. EXPERIMENTAL STUDY OF INDUCTION-COUPLED LIQUID-METAL MAGNETOHYDRODYNAMIC CHANNEL FLOW

The direct generation of electrical power from the kinetic power carried by an electrically conducting fluid may be achieved through the utilization of the inductive coupling

between a traveling magnetic field and the moving fluid. It has been shown[1] that the operating characteristics of an MHD induction generator can be determined from the magnetic Reynolds number, based on wave speed and velocity and the velocity difference between the wave and the fluid. The conductivity and velocity attainable with ionized gas flows are too low to yield satisfactory operating conditions, but liquid metals yield more promising results as is indicated in Table XVII-1. Two methods of converting the thermal energy of a power-system heat source to the kinetic energy of a moving fluid have recently been proposed.[2,3]

Table XVII-1. Experimental results.

		Liquid Metal	Metal Vapor
velocity	v	10^2	10^3 m/sec
conductivity	σ	10^6	10^2 mhos/m
magnetic field	B	2	2 wb/m^2
power density	$\frac{1}{4}\sigma v^2 B^2$	10^{10}	10^8 W/m^3
wavelength	λ	50	50 cm
magnetic Reynolds number	$\frac{\mu\sigma v\lambda}{2\pi}$	10	10^{-2}

The magnetic Reynolds number criterion used in Table XVII-1 is attained from a one-dimensional analysis that ignores real machine effects, all of which may be expected to degrade performance. An induction-coupled liquid-metal MHD channel flow has been set up to investigate directly real machine effects such as end losses, fluid viscous losses, magnetic-field configuration, and edge effects. Eutectic sodium potassium alloy (NaK) was selected as the working fluid for a closed-loop flow facility driven by a positive displacement pump with a capacity of 20 gallons per minute at a head of 20 p.s.i. A 300 gallon per minute centrifugal pump will be obtained for future experiments. The entire flow loop is fabricated from stainless steel with neoprene connectors and O-rings. Figure XVII-11 shows the general layout of the flow facility, including the instrumentation used for the experimental study. Details of the design and construction of the loop have already been given.[4-6]

The traveling-field coil system is contained in the horizontal cylindrical tank on the table shown in Fig. XVII-11. It comprises 24 pairs of saddle coils assembled around a 4 1/4 inch diameter tube as shown in Fig. XVII-12. The coil pairs are spaced 6 inches

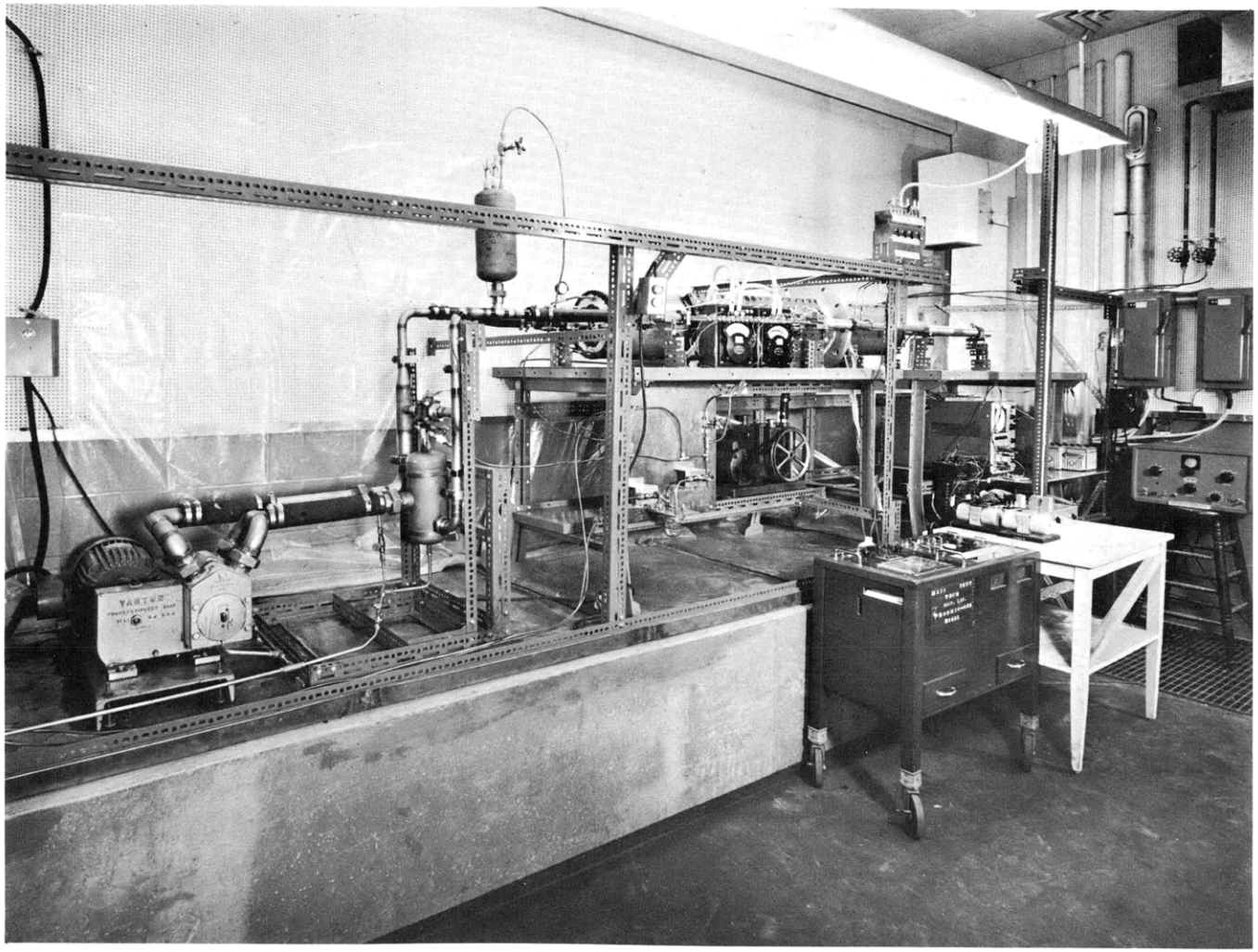

Fig. XVII-11. Liquid-metal flow facility.

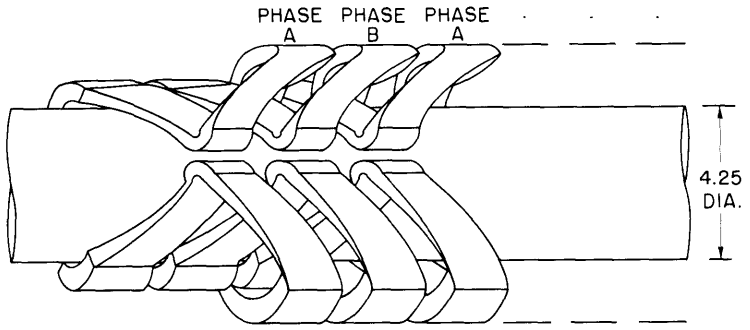

Fig. XVII-12. Traveling-field coil structure.

apart, and are connected to produce a two-phase system with a wavelength of 1 ft. The coil structure is kerosene-cooled, and powered from a 60-cps alternator rated at 44 kva at 230 volts. A variable-speed DC motor drive enables the alternator frequency to be varied.

A high aspect ratio rectangular channel was used in these experiments. The internal dimensions were 2 3/4 in. × 3/8 in. which yielded a velocity of approximately 10 ft per second at maximum capacity. The long sides of the channel were insulated with epoxy but, to minimize electrical losses in the chosen geometry, the remaining two sides of

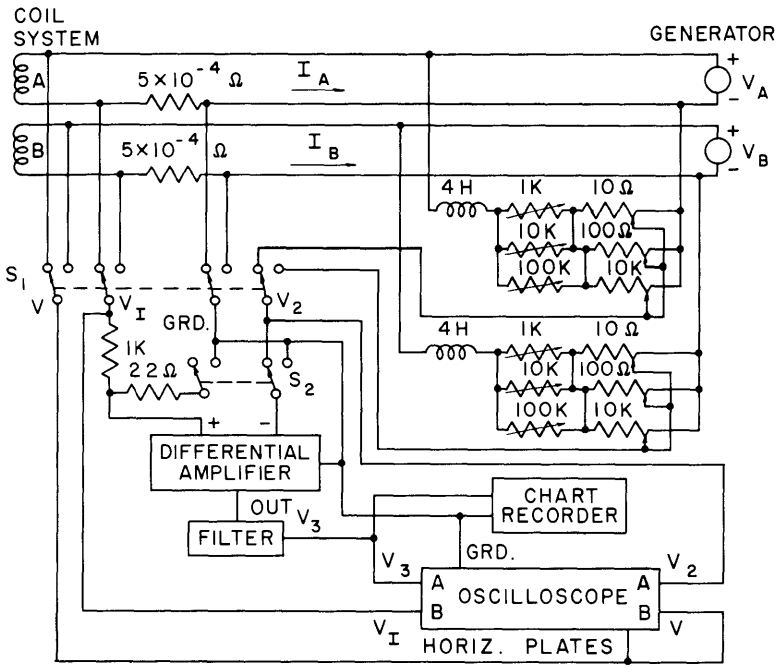

Fig. XVII-13. Power-flow measurement circuit details.

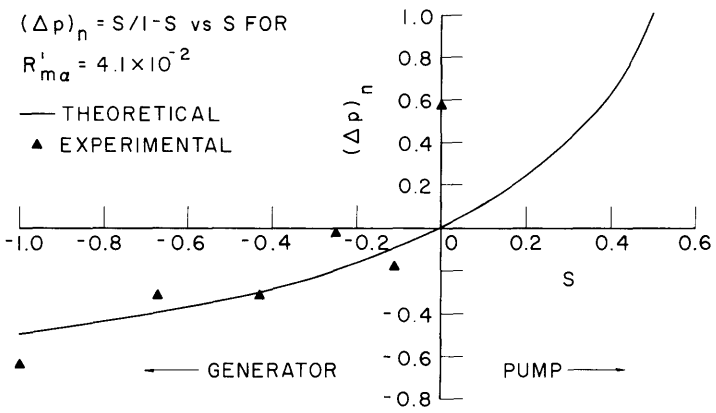

Fig. XVII-14. Normalized pressure vs slip.

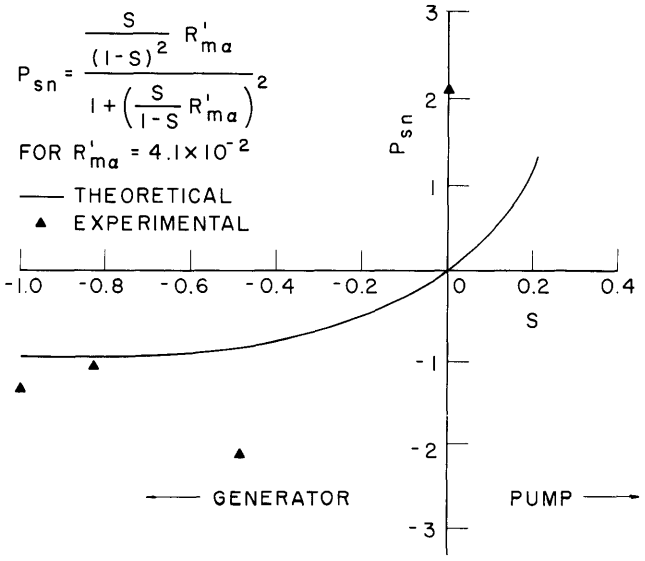

Fig. XVII-15. Normalized power vs slip.

the channel were of nickel-plated copper. Transition sections were provided at each end of the generator channel to connect to the 1.1 in. flow-loop tubing. Provision was made for fluid pressure to be measured at 6-inch intervals along the channel.

Measurements were made of fluid velocity, pressure drop along the MHD channel section, and power flow between the alternator and the coil system. The system was first filled with alcohol to check out operation and calibrate the venturi flowmeter. To minimize flow pulsations introduced by the positive displacement pump, the fluid velocity was kept at maximum value throughout runs with NaK, and the slip between the field and the fluid was varied by adjusting the speed of the alternator drive motor. Direct-reading NaK manometers did not function satisfactorily, and so a single mercury

manometer was used. This was connected by a system of valves to the appropriate pressure measurement point.

Because of the small amount of electrical power flow involved in the MHD interaction, relative to the 1500 volts required to drive the field coils, direct measurement of power flow could not be made. Instead, the differential amplifier scheme shown in Fig. XVII-13 was used, and was calibrated directly by means of dummy loads connected across the coil terminals. Pressure-slip and power flow-slip data are given in Figs. XVII-14 and XVII-15, respectively, and a comparison with theoretical predictions is made.

The normalization of the experimental results and the theoretical curves are obtained in the following way. The power P_s delivered by the fluid to the coils[7] is given by

$$P_s = \frac{\mu_o c \lambda N^2 I^2}{K + \alpha} \frac{v_s s R_{m\alpha}}{1 + s^2 R_{m\alpha}^2}, \tag{1}$$

where μ_o is the fluid permeability, λ is the wavelength, v_s is the wave speed, NI is the magnetomotive force, c is the over-all width of the machine, and

$$s = 1 - v/v_s \tag{2a}$$

$$R_{m\alpha} = \frac{\mu_o \sigma_f a v_s}{K + \alpha} \tag{2b}$$

$$\alpha = ak \tag{2c}$$

$$K = \frac{\mu_o}{\mu_c}. \tag{2d}$$

In these definitions, s denotes the slip between v_s and the average fluid velocity v; $R_{m\alpha}$ is the relevant magnetic Reynolds number; σ_f, the fluid conductivity; a, the channel half-width; K, the ratio giving μ_o to the field-structure permeability μ_c; and α, the ratio that is a measure of the ratio of a to λ in terms of the wave number k.

As the experimental results are for a constant value of v, and the effect of changing $sR_{m\alpha}$ is of interest, it is convenient to define a constant value of magnetic Reynolds number $R'_{m\alpha}$ as

$$R'_{m\alpha} = R_{m\alpha} \frac{v}{v_s} = \frac{\mu_o \sigma_f a v}{K + \alpha}. \tag{3}$$

The normalized power P_{sn} is then obtained as

$$P_{sn} = \frac{P_s(K+a)}{\mu_o c\lambda (NI)^2 v} = \frac{\frac{s}{(1-s)^2} R'_{ma}}{1 + \left(\frac{s}{1-s}\right)^2 (R'_{ma})}. \tag{4}$$

For the experimental conditions, $R'_{ma} = 0.041$.

In a similar fashion, the pressure change along the channel,[7] Δp, is given by

$$\Delta p = \frac{\mu_o N^2 I^2 L}{2a(K+a)} \frac{sR_{ma}}{1 + s^2 R_{ma}^2}, \tag{5}$$

and the normalized $(\Delta p)_n$ is

$$(\Delta p)_n = \Delta p \frac{2a(K+a)}{L\mu_o (NI)^2} = \frac{\frac{s}{1-s} R'_{ma}}{1 + \left(\frac{s}{1-s}\right)^2 (R'_{ma})^2}. \tag{6}$$

For the region of experimental interest,

$$\left(\frac{sR'_{ma}}{1-s}\right)^2 \ll 1 \tag{7}$$

and

$$(\Delta p)_n \approx \frac{s}{1-s}. \tag{8}$$

The correlation of theory with experiment in Figs. XVII-14 and XVII-15 is quite satisfactory when the difficulty of measuring values of P_s less than 0.5 watt is taken into account. It should be noted that the sign of both the pressure drop and power flow indicates generator action in the region of negative s, and shows that electrical losses resulting from end effects, etc., were not of sufficient magnitude to absorb the generated power. Because of the very low Hartmann number involved, fluid losses for the interaction region were estimated by using ordinary friction factor curves to the 21.31 watts for v = 10 ft per second. This is in good agreement with the measured value of 22.2 watts, and confirms the prediction that ordinary friction losses are the predominant effect in this experiment. The experimental apparatus is now being modified to obtain the stronger magnetohydrodynamic interactions that are evidently required for further study of induction-coupled flows.

W. D. Jackson, R. P. Porter

References

1. W. D. Jackson and E. S. Pierson, Operating Characteristics of the MPD Induction Generator, Magnetoplasmadynamic Electrical Power Generation, I.E.E. Conference Report Series No. 4, 1963.

2. W. D. Jackson, Review of MHD Power Generation, Proc. AMU-ANL Conference on Direct Energy Conversion, Argonne National Laboratory, Lemont, Illinois, November 1963.

3. D. G. Elliot, Two-fluid magnetohydrodynamic cycle for nuclear-electric power conversion, Am. Rocket Soc. J. 32, 924 (1962).

4. F. W. Fraim IV, Design and Construction of a Magnetohydrodynamic Channel Flow System, S. B. and S. M. Thesis, Department of Electrical Engineering, M. I. T., 1962.

5. J. F. Carson, Friction Factor Measurement for NaK Magnetohydrodynamic Channel Flow, S. B. Thesis, Department of Electrical Engineering, M. I. T., 1963.

6. M. H. Reid, Experimental Investigation of a Liquid Metal Induction Generator, S. M. Thesis, Department of Electrical Engineering, M. I. T., 1963.

7. E. S. Pierson, Power flow in the magnetohydrodynamic induction machine, Quarterly Progress Report No. 68, Research Laboratory of Electronics, M. I. T., January 15, 1963, pp. 113-119.

E. NEURAL PATTERNS IN BLOOD-PRESSURE REGULATION*

This study is concerned with the description of a part of the pressoreceptor reflex system, a biological control system involved in the regulation of blood pressure. The system consists of stretch-sensitive receptors located in the walls of certain arteries which transduce the pressure signal into related electrical activity on the nerve associated with the sensors; the nerve itself, which transmits the information to the brain; the vasomotor center of the brain, which processes the information; and the efferent nerves, which transmit the control signals to the heart and blood vessels, thereby closing the control loop.

The work reported on here deals with the transduction of the pressure signals into nerve firings on the nerve involved. Specifically, the relation between the firing frequency on the carotid sinus nerve and the pressure at the carotid sinus is considered. From the published data of single-fiber studies, it is possible to construct a model that qualitatively at least reproduces the behavior of the biological system.

The static behavior of the system is characterized by no neural activity below a threshold level of pressure, a firing rate proportional to pressure above the threshold value, and an asymptotic approach to a maximum firing frequency as the static pressure is raised to a sufficiently high level.

The dynamic response of the system, as determined by the system response to step-like variations in pressure, exhibits a rapid increase of firing rate upon application of a positive step which is followed by a decay to a final value that is higher than the value of

*This work was supported in part by the National Institutes of Health (Grant No. 5 TI HE 5550-02.

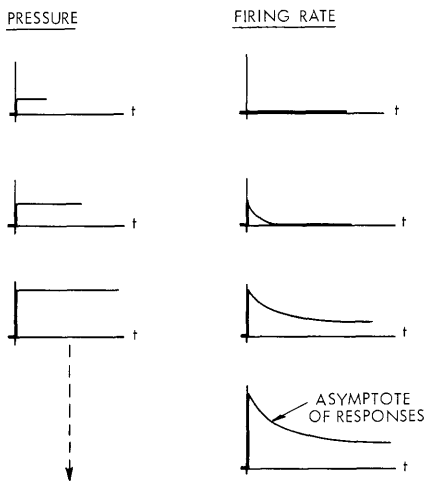

Fig. XVII-16. Step responses on a single fiber.

firing rate before application of the step. A negative step produces an initial cessation of firing, after which the firing rate grows back to a steady value lower than its initial value.

If the pressure steps are started at 0 mm Hg and their amplitude is increased, the (idealized) responses are observed as shown in Fig. XVII-16. These observations, as well as observations of ramp responses, suggest that the system may be modeled in the manner of Fig. XVII-17. The first nonlinear section results in the successive step responses approaching an asymptotic response. The use of the linear filter corresponds to approximating the step response by the sum of a step and a single decaying exponential. The effect of the second nonlinear section corresponds to that of the static threshold and accounts for the nature of the responses to negative steps.

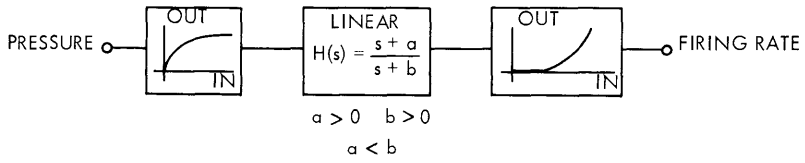

Fig. XVII-17. Model whose response approximates the response of a single fiber.

The complexity of this model can be increased by adding more poles and zeros (approximating the step response by sums of decaying exponentials).

The experimental part of this study consisted of the application of (almost) sinusoidal pressure variations imposed upon static levels of pressure, and the recording of the resultant activity on the carotid sinus nerve. The recordings were obtained from multifiber preparations. The activity corresponding to 10 cycles of each stimulus frequency at each static level was recorded, so that some averaging could be performed to reduce the effects of noise (noncorrelated) components in the outputs.

The data-reduction scheme consists of thresholding the outputs to obtain a clean base line, and counting the number of firings in a window whose position with respect to the stimulus is controllable, as indicated in Fig. XVII-18. Using this scheme, we obtained curves of firing rate vs time corresponding to the stimulation; a typical example appears

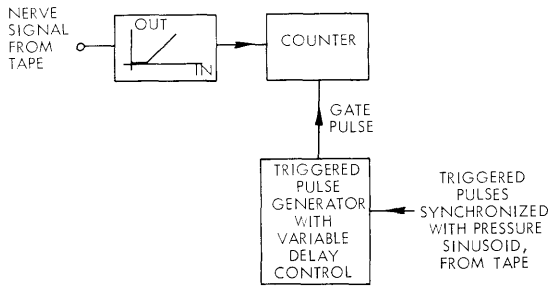

Fig. XVII-18. Block diagram of data reduction scheme.

in Fig. XVII-19. Qualitatively, the peaks of these curves tend to occur in the region in which the corresponding pressure is near its peak. Since these curves are not sinusoidal, their first harmonics are being calculated, and the amplitude and phase of the first harmonics with respect to the amplitude and phase of the pressure are being examined. Preliminary results indicate that the angle of the system function (angle of first harmonic of averaged firing rate vs time minus angle of pressure) is positive. This agrees with the fact that the coefficients of the decaying exponentials used to approximate the step response are positive, that is, that the residues in the poles of H(S) are positive, which implies that

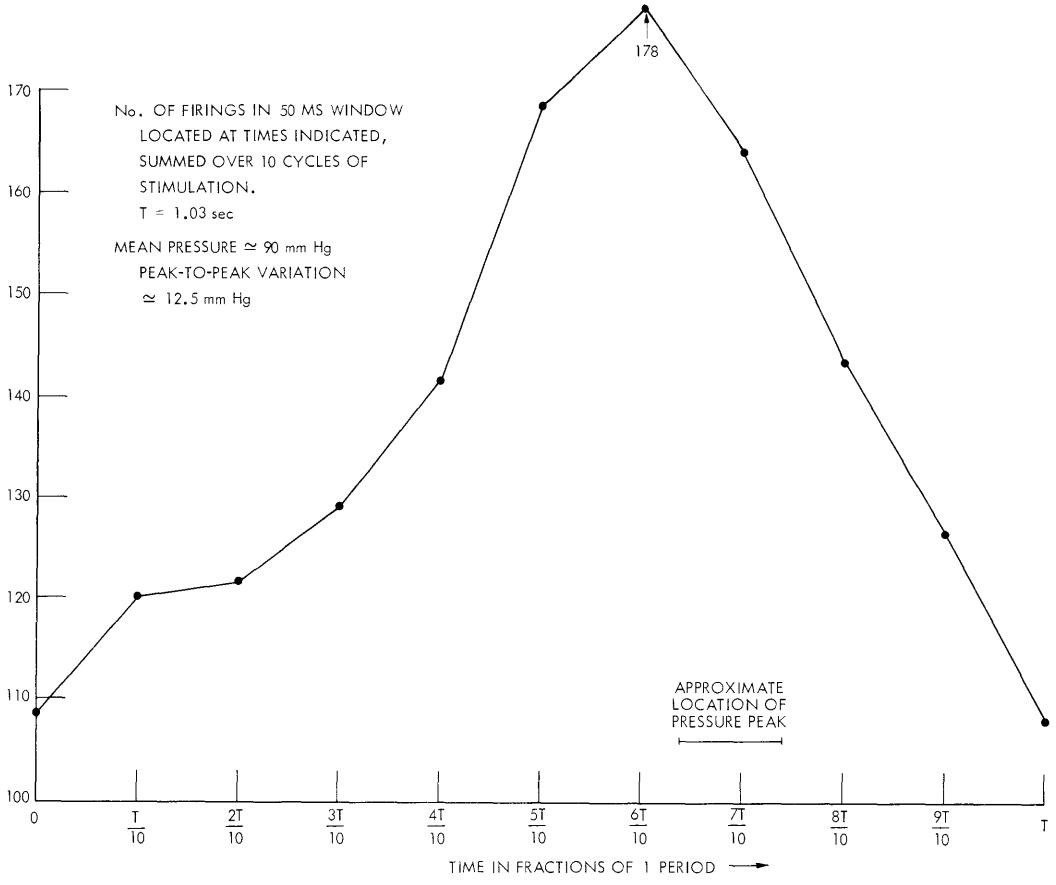

Fig. XVII-19. Typical experimental curve of firing rate vs time obtained from gross recordings.

the negative real poles and zeros of H(S) alternate, with a zero nearest the origin. Requiring the critical frequency nearest the origin to be a zero, together with requiring the number of poles to equal the number of zeros, implies positive phase shift.

These preliminary results also indicate that the system gain (amplitude of first harmonic of the averaged firing rate versus time divided by amplitude of the pressure sinusoid) is an increasing function of frequency. This trend agrees with the amplitude vs frequency behavior of the system function $H(S) = \frac{s + a}{s + b}$, $0 < a < b$.

D. H. Pruslin

F. PENETRATION OF AN ION THROUGH AN IONIC DIPOLE LAYER AT AN ELECTRODE SURFACE

When cesium is adsorbed on a metallic surface in the form of ions, these ions and their images form a dipole layer.[1,2] If an ion is introduced to the surface, it travels through a fraction f of the potential difference caused by this dipole layer from the image plane to a point at infinity,[2] as shown in Fig. XVII-20. Values of the penetration

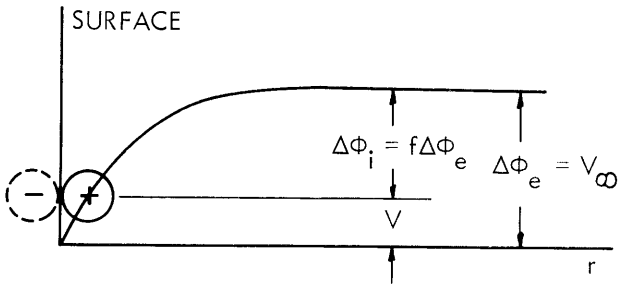

Fig. XVII-20. Potential of an ion with respect to the potential of a substrate surface as a function of distance from the surface.

coefficient have been computed by Rasor and Warner[3] and by Kennedy.[4] In this report it is shown that the penetration coefficient can be evaluated as a function of coverage in two different ways, one for an immobile film, and the other for a completely mobile film. Subsequently, values of the penetration coefficient can be obtained from the Langmuir-Taylor data for cesium on tungsten in two different ways. Both methods give values for the penetration coefficient which agree closely with each other over the entire range of the coverage, and these values fall between the theoretical expressions for f obtained for the cases of immobile and mobile films.

1. Penetration Coefficient for an Immobile Film

For an immobile film the cesium ions occupy fixed lattice sites, as shown in Fig. XVII-21a. A cross-section view of the surface is shown in Fig. XVII-21b. The following nomenclature is used.

Symbol	Definition
d	lattice constant of the crystal
λ	distance of the center of charge of an adsorbed ion from the image plane, taken to be equal to the hard-core ionic radius of cesium
r	distance of an ion from the image plane
r_{ij+}	distance between an ion at r and any adsorbed ion at i,j
r_{ij-}	distance between an ion at r and an image of any adsorbed ion at i,j
r_{ij}	distance between an adsorption site and any other site at i,j
$\theta_i = \frac{\sigma_i}{\sigma_1}$	ionic coverage
$\sigma_1 = \frac{1}{4d^2}$	surface density of adsorbates at full coverage

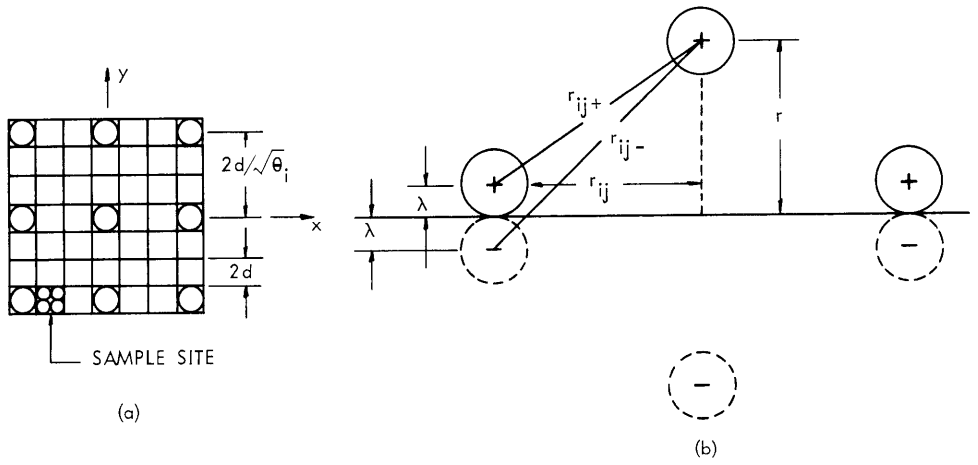

Fig. XVII-21. (a) Immobile adsorbate-substrate system. (b) Cross section of adsorbate-substrate system.

The potential on an ion at any r as a result of being in the field of the remaining adsorbed ions and their images can be expressed as

$$V(r) = q \sum \left(\frac{1}{r_{ij+}} - \frac{1}{r_{ij-}} \right), \tag{1}$$

in which the summation is performed over every adsorbate, and each adsorbate corresponds to a distinct distance r_{ij}. For the square lattice model with perfect arrangement of adsorbates,

$$r_{ij+}^2 = (r-\lambda) + r_{ij}^2 \tag{2a}$$

$$r_{ij-}^2 = (r+\lambda) + r_{ij}^2 \tag{2b}$$

with

$$r_{ij}^2 = \frac{4d^2}{\theta_i}(i^2+j^2). \tag{2c}$$

Equation 1 is rewritten

$$V(r) = q \sum \frac{r_{ij-} - r_{ij+}}{r_{ij+}r_{ij-}} \frac{(r_{ij-}+r_{ij+})}{(r_{ij-}+r_{ij+})}$$

or

$$V(r) = q \sum \frac{r_{ij-}^2 - r_{ij+}^2}{r_{ij+}r_{ij-}^2 + r_{ij+}^2 r_{ij-}}. \tag{3}$$

Substituting Eq. 2 in Eq. 3, for $r = \lambda$, yields

$$V(r=\lambda) = 4q\lambda^2 \sum_{-\infty}^{\infty}\sum \frac{1}{\left[4\lambda^2 + \frac{4d^2}{\theta_i}(i^2+j^2)\right]\left[\frac{4d^2}{\theta_i}(i^2+j^2)\right]^{1/2} + \left[4\lambda^2 + \frac{4d^2}{\theta_i}(i^2+j^2)\right]^{1/2}\left[\frac{4d^2}{\theta_i}(i^2+j^2)\right]} \tag{4}$$

in which i,j take on all values except $i = j = 0$.

Since $\lambda^2 \ll \frac{d^2}{\theta_i}(i^2+j^2)$, we neglect λ^2 in the denominator of Eq. 4 to obtain

$$V(r=\lambda) = \frac{q\lambda^2\theta_i^{3/2}}{4d^3} \sum_{-\infty}^{\infty}\sum \frac{1}{(i^2+j^2)^{3/2}}. \tag{5}$$

Evaluating the sum[5] then gives the potential of an adsorbed ion resulting from the other adsorbed ions, in other words, the value of V in Fig. XVII-21b, which is equal to

$$V(r=\lambda) = \frac{2.21q\lambda^2}{d^3}\theta_i^{3/2}. \tag{6}$$

The potential at infinity with respect to the image surface is identified as V in Fig. XVII-20. For large r, the potential felt by an ion from the discrete dipoles is

approximately the same as that which would be felt from a continuously distributed dipole layer. This value has been stated[1,6] to be

$$\lim_{r\to\infty} V = V_\infty = 2\pi M\sigma_1\theta_i \qquad \text{for } M = 2q\lambda. \tag{7}$$

2. Mobile Films

For mobile films the cesium ions can move freely from one lattice site to another, and hence each lattice site has the same probability of being occupied by a cesium ion that is simply the coverage. Hence

$$p(\theta) = \theta. \tag{8}$$

The potential, then, of an ion at distance r is obtained by summing over each lattice site and multiplying this potential by the probability of occupation. For the mobile film, $r_{ij}^2 = 4d^2(i^2+j^2)$, so that

$$V(r=\lambda) = \frac{q\lambda^2}{4d^3} \sum_{-\infty}^{\infty}\sum \frac{P(\theta)}{(i^2+j^2)^{3/2}}. \tag{9}$$

Evaluating the sum gives

$$V(r=\lambda) = \frac{2.21q\lambda^2\theta_i}{d^3}. \tag{10}$$

3. Determination of f

The penetration coefficient is determined by the relation $f = \frac{\Delta\phi_i}{\Delta\phi_e}$, where $\Delta\phi_i$ is the change of ionic work function, and $\Delta\phi_e$ is the change of electron work function. The increase in ionic work function occurs because the ion penetrates through the potential $V_\infty - V$ of Fig. XVII-20. Thus $\Delta\phi_i = V_\infty - V$. The electron work function decreases as a result of the accelerating potential V_∞, so that $\Delta\phi_e = V_\infty$. Thus we obtain the relation

$$f = 1 - \frac{V}{V_\infty}. \tag{11}$$

Substituting the calculated values for V and V_∞, we obtain for the immobile film

$$f_{im} = 1 - \frac{2.21\lambda^\infty}{\pi d}\,\theta_i^{1/2} = 1 - 0.362\theta_i^{1/2}. \tag{12}$$

For the completely mobile film independent of coverage,

$$f_m = 1 - \frac{2.21\lambda}{\pi d} = 0.632. \tag{13}$$

4. Ionic Coverage

The ionic coverage is related to the total coverage by Fermi-Dirac statistics, and the following relation has been derived.[7]

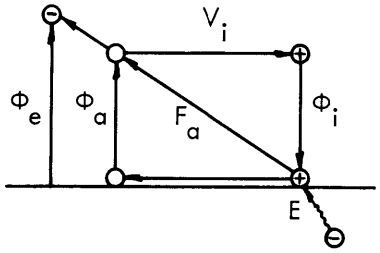

Fig. XVII-22. Born-Haber cycle.

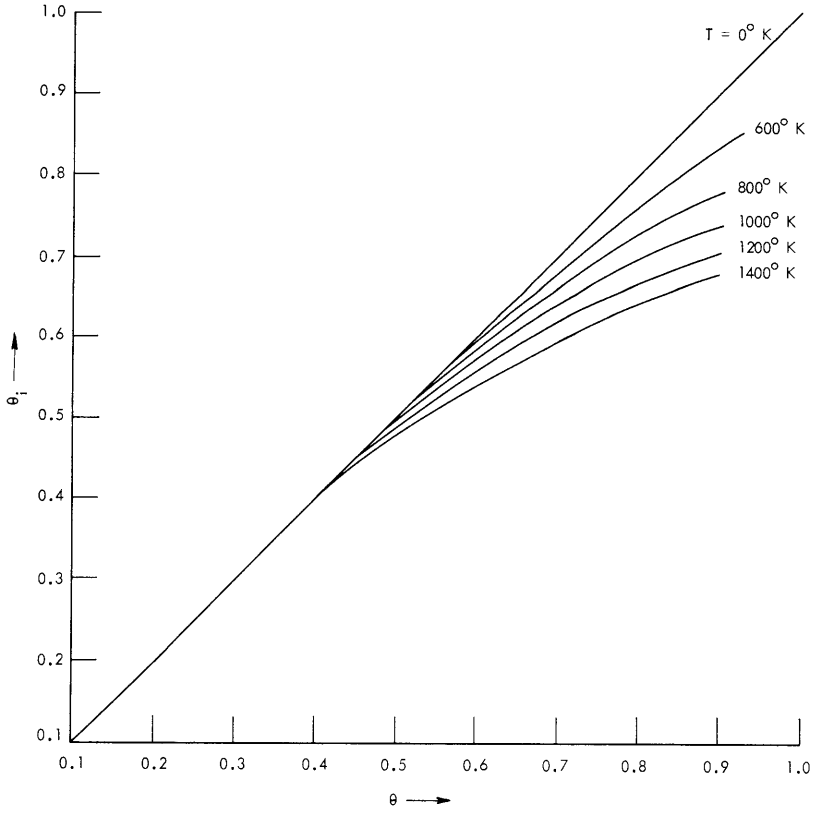

Fig. XVII-23. Ionic coverage vs total coverage for various surface temperatures.

$$\theta_i = \frac{\theta}{1 + \exp(-E/kT)}, \tag{14}$$

where E is the difference in energy between a bound 6S electron of a surface adsorbate atom and the Fermi level of the substrate. This quantity is determined from experiment in the following manner. Consider the Born-Haber cycle of Fig. XVII-22. Two energy balances result from this cycle:

$$f_a = \phi_e - V_i + \phi_i \tag{15}$$

and

$$f_a = \phi_a + E. \tag{16}$$

Equation 15 can be solved for f_a by using the atomic heat of adsorptions data of Taylor and Langmuir.[2] If it is assumed that ϕ_a does not change with coverage – which is reasonable since the atom is not acted upon by the electric forces of the dipole layer – and if f_a for various materials tends towards the same value at higher coverages, then knowing $f_a = f_a(\theta)$ and ϕ_a, we can calculate the value of $E = E(\theta)$ and substitute it in Eq. 13; this procedure yields $\theta_i = \theta_i(\theta)$. This is plotted for various temperatures in Fig. XVII-23 for cesium tungsten.

5. Correlation of Experimental Results

Theoretical values for f from Eqs. 11 and 12, for the two limiting cases of mobile and immobile films, are plotted against θ in Fig. XVII-24. Curves are also drawn on the same coordinates by computing $f = \frac{\Delta\phi_i}{\Delta\phi_e}$ from previous experimental data.[2,8] The values of f computed from Taylor-Langmuir data fall between the theoretical values obtained for the two limiting cases considered. Furthermore, values of f calculated in two different ways from the Taylor-Langmuir measurements agree within experimental uncertainties. Curve 4 is calculated from direct measurement of ϕ_i. By using the cycle of Fig. XVII-22, together with the relations

$$\phi_i(\theta) = \phi_{io} + \Delta\phi_i, \tag{17}$$

$$-\Delta\phi_e = \phi_e - \phi_{eo}, \tag{18}$$

$$\Delta\phi_i = f\Delta\phi_e, \tag{19}$$

so that

$$\phi_i(\theta) = \phi_{io} + f(\phi_{eo} - \phi_e) \tag{20}$$

(where the zero subscripts denote values at zero coverages), the expression for f is obtained.

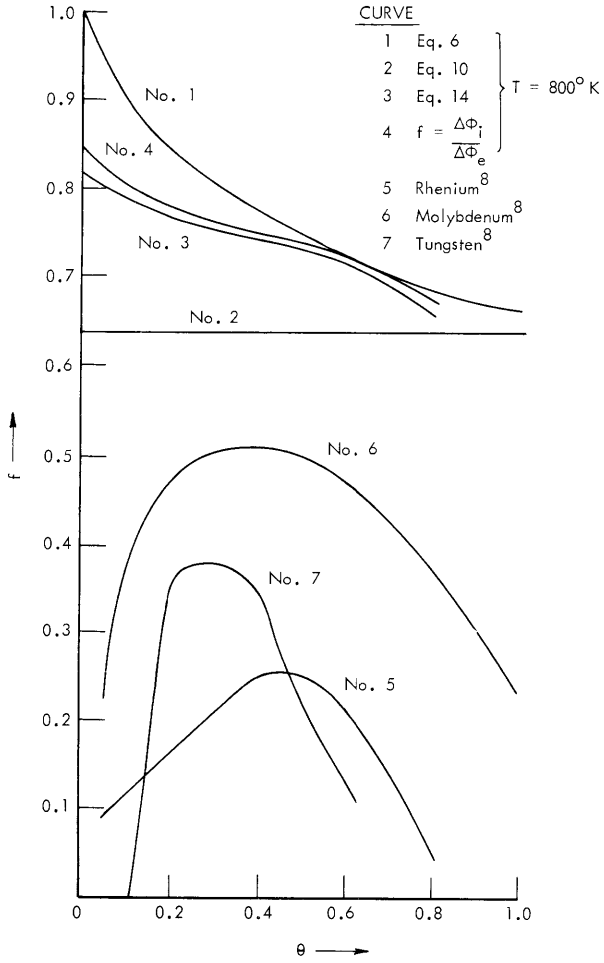

Fig. XVII-24. Penetration coefficient vs coverage.

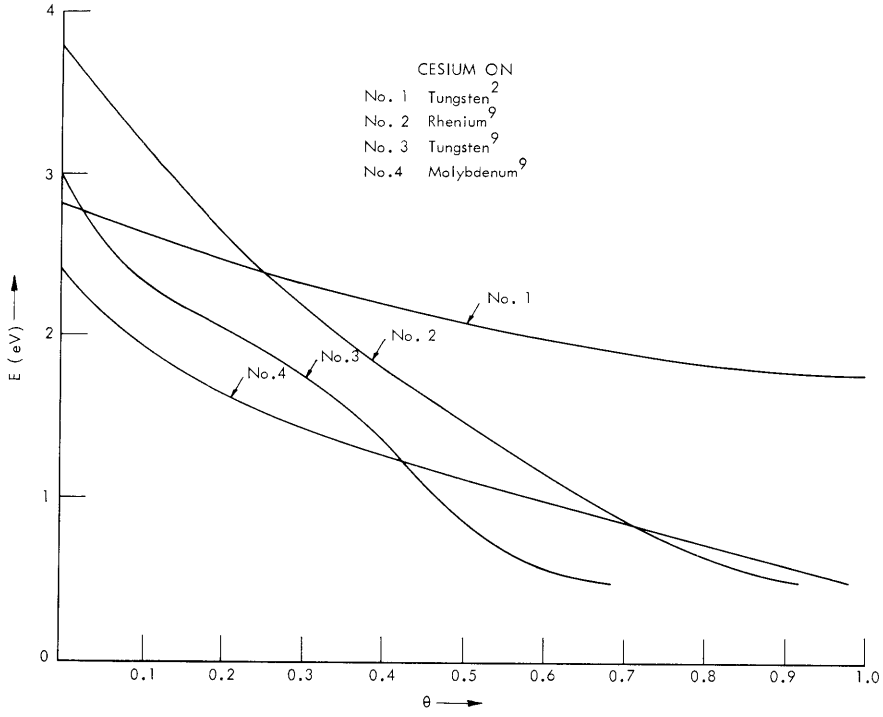

Fig. XVII-25. Atomic heater adsorption vs coverage.

Table XVII-2. Experimental values of relevant potentials and penetration coefficients.

θ	E(0)eV	ϕ_e(eV) (measured)	$\Delta\phi_e$(eV)	ϕ_i(eV) (measured)	ϕ_i(eV)	f_a(eV) (measured)	Curve 3 f (computed)	Curve 4 f (computed)
0	1.1	4.62	0	2.05	0	2.82		
.05	.99	4.12	.5	2.46	.41	2.72	.80	.82
.1	.90	3.75	.87	2.76	.71	2.63	.782	.817
.2	.73	3.10	1.52	3.22	1.17	2.47	.77	.77
.3	.58	2.62	2.0	3.58	1.53	2.32	.75	.765
.4	.45	2.20	2.42	3.87	1.82	2.19	.739	.751
.5	.34	1.89	2.73	4.06	2.01	2.09	.733	.737
.6	.26	1.74	2.88	4.13	2.08	1.98	.704	.723
.7	.205	1.70	2.92	4.07	2.02	1.90	.685	.693
.8	.165	1.78	2.84	3.96	1.91	1.84	.655	.673

$$f = \frac{f_a + V_i - \phi_{io} - \phi_e}{\phi_{eo} - \phi_e}. \tag{21}$$

Equation 17 is used with the Taylor-Langmuir measurements of $f_a = f_a(\theta)$ to calculate curve 3. This double agreement increases the confidence placed in the Taylor-Langmuir data. Table XVII-2 lists the numerical values used in the calculations.

The results of Charbonnier and others[8] for the variation of the energy of adsorption with coverage are shown in Fig. XVII-25. From this figure it is seen that there is a much stronger variation of the energy of desorption with coverage; this result is in disagreement with the Taylor-Langmuir data. In Fig. XVII-24, the penetration coefficient as obtained from Eq. 17, with data of Charbonnier, Swanson, Cooper, and Strayer[8] used, is also shown. The values obtained for f versus coverage do not fall between the two limiting cases of mobile and immobile films, as do the values obtained from Taylor-Langmuir data.

J. W. Gadzuk

References

1. I. Langmuir, J. Am. Chem. Soc. 54, 2798 (1932).

2. J. B. Taylor and I. Langmuir, Phys. Rev. 44, 423 (1933).

3. N. S. Rasor and C. Warner III, Correlation of Electron, Ion and Atom Emission Energies, Atomics International Report AI-6799, November 1961.

4. A. J. Kennedy, Adv. Energy Conv. 3, 207-222 (1963).

5. J. Topping, Proc. Roy. Soc. (London) A114, 67 (1927).

6. J. H. de Boer and C. F. Veenemans, Physica 1, 953-965 (October-November 1934).

7. E. N. Carabateas, Analytical Description of Cesium Films on Metal, Report to the National Science Foundation, "Basic Studies of Cesium Thermionic Converters," June 1963.

8. F. M. Charbonnier, L. W. Swanson, E. C. Cooper, and R. P. Strayer, Investigations of the Migration, Desorption, and Voltage Breakdown Properties of Cesium Films on Refractory Electrodes, Field Emission Corporation Report Log. No. 63020, April 1963.